Performance Analysis of Induction Motor based PV Feed Water Pumping System with Small Signal Analysis

Gaurav Shukla, Vishal Sharma, Ramachandran T and Rajesh Guputa

Gaurav Shukla, Assistant Professor, Maharishi School of Engineering & Technology, Maharishi University of Information Technology, Uttar Pradesh, India, Email Id- gaur.knit@gmail.com
Vishal Sharma, Assistant Professor, Mechanical Engineering, Vivekananda Global University, Jaipur, India, Email Id-vishal_sharma@vgu.ac.in
Dr. Ramachandran T, Professor, Department of Department of Mechanical Engineering, Faculty of Engineering and Technology, Jain (Deemed-to-be University), Bangalore, Karnataka, India, Email Id -t.ramachandran@jainuniversity.ac.in,
Mr. Rajesh Guputa, Pro Chancellor, Department of Management, Sanskriti University, Mathura, Uttar Pradesh, India, Email Id- prochancellor@sanskriti.edu.in

Abstract: Photovoltaic (PV) powered water pumping systems utilizing induction motors are becoming increasingly popular in different regions. The lack of storage devices in the system enhances its cost-efficiency. Efficient energy management is crucial for maintaining power balance within the system, and this can be achieved through the implementation of an effective control technique. A small signal analysis is performed to optimize the parameters of the controllers used in order to analyze the system. The dynamic behavior of the PV-based water pumping system, which is powered by an induction motor and regulated by a vector controller, is analyzed by converting its non-linear model into a linear model. The paper discusses the design of parameters for two PI controllers utilized to regulate the PV terminal voltage and motor speed, based on the transfer function derived from the linear model. The study also showcases the small signal function's reaction through MATLAB, with adjustments made to the reference dc-link voltage. Additionally, a comprehensive step-by-step mathematical analysis is included to enhance the overall understanding and analysis of the system.

Keywords: PV, Small Signal Analysis, Water Pumping System, Induction Motor Drive.

Corresponding Author: gaur.knit@gmail.com

1. INTRODUCTION

Rural electrification poses significant challenges in practical implementation. Many rural areas across the globe lack access to electricity through the main power grid, which hampers their development. However, the use of renewable energy sources for generating electricity can address this issue and also contribute to mitigating global warming. Among the various applications of standalone photovoltaic (PV) systems, water pumping plays a crucial role. To ensure optimal performance of the water pump, an efficient maximum power point tracker (MPPT) system is essential. In PV-fed water pumping systems (WPSs), under few kW pumps are commonly employed to lift water from underground sources for small-scale and drip irrigations, and household needs. While a PV-powered WPS with a DC motor is already operational, it is associated with high maintenance and costs. Therefore, considering an induction motor (IM) for powering WPSs could be a viable alternative.

Solar irradiation is the primary source of power for PV panels, which in turn generate discharged water in the WPS. To optimize power generation, the voltage across the PV panel must be adjusted based on the reference signal (Vref or V*dc) provided by the perturb and observe (P&O) algorithm. Sun irradiation plays a significant role in this process. Additionally, the volume of water sprayed is influenced by the overall head and speed of the IM. A closed loop control is crucial for efficient management of the power generated by the PV system and consumed by the IM. In this study, a vector controller is employed to drive an IM connected directly to a water pump. In some cases, the pumping head (H) can be considered an additional input variable, representing the motor's torque. The power required by the motor is influenced by factors such as the load, excitation voltage, and frequency. Vector control is particularly beneficial for pumping applications as it helps reduce torque ripples compared to v/f control. Centrifugal pumps are commonly utilized in agricultural settings.

The elimination of batteries in the design of a PV based WPS can lead to cost savings and eliminate the need for maintenance. To avoid the use of an additional converter for the PV system's MPPT, the inverter itself is utilized to regulate the dc-link voltage, which is achieved through the P&O algorithm and inverter control. Consequently, a separate dc-dc converter is not required for MPPT. Centrifugal pumps are widely employed in agriculture. The aim of this research is to produce advantages for appropriate PI controllers and to carry out small signal analysis.

The proposed system, as shown in Figure 1, comprises of a PV, inverter, pump, and IMs. This study focuses on the analysis of a small signal for an efficient IM control in order to regulate a WPS that is powered by PV.

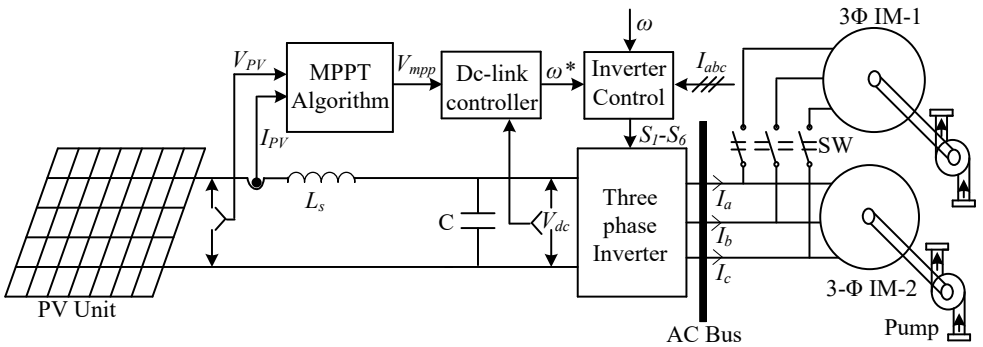

Fig. 1: IM driven WPS fed by PV.

2. PUMPING PROCESS

PV-powered water pumping equipment is a common feature in distributed energy systems. To supply the necessary alternating current to the induction motor (IM), a three-phase inverter is essential. In this study, the vector controller is employed to generate the appropriate gate-signals for the 3-phase inverter. The IM is directly connected to a centrifugal pump, which draws water from underground and delivers it to the outlet. The vector control method effectively separates the torque and flux controls, ensuring efficient electricity consumption by the motor. The market offers a wide variety of motor-pump sets suitable of WPSs. For lifting water from depths exceeding 400 feet, typically utilize IMs coupled centrifugal pumps. In PV shallow water pumping applications with low head requirements, single-stage centrifugal pumps are more commonly used compared to other type of pumps [8].

Centrifugal pumps achieve optimal performance when the head and flow rate are aligned with a curve corresponding to the motor's designated speeds. The speed of the engine directly influences the rate at which water is flows. Moreover, the relationship between the speed's square and cube and the head and hydraulic power is inversely proportional. A minimum cutoff speed is required in order to start the water discharge from the outlet. When the pump surpasses a certain threshold or base value (t) in terms of speed, the flow rate of water (Q, liter/min) changes proportionally with the speed, as shown in equation (1) and determined through curve fitting [9].
$Q = 0$, if $\omega < \omega_t$. and $Q = a\omega\text{-}b$, if $\omega \geq \omega_t$

3. IM SPEED CONTROL

Reference frequency of the motor (F*) in the projected control system is determined using a proportional plus integral (PI-1) approach, based on the difference between Vdc and Vmpp or Vref. The reference speed (ω*) is calculated by multiplying F* by 120/P (where P represents the number of poles of the IM). As shown in Figure 2, a limiter is applied to limit the ω* produced by the PI-1 controller to limit the speed within a specified range. The input signal for vector control is the allowed speed (constrained by the limiter), and vector control generates the signals to S1-S6 for the inverter. F_{max} denotes the highest permissible frequency, which corresponds to the utmost attainable speed.

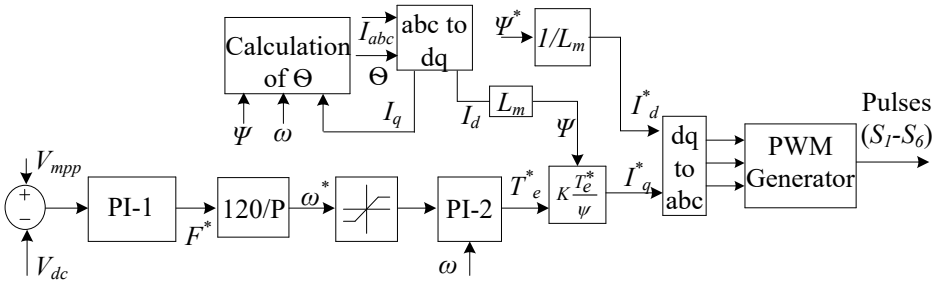

Fig. 2: Proposed Speed control of motor.

4. SMALL SIGNAL MODELING

Due to the close proximity of generators and load within a system, the analysis of oscillations, transient stability, and voltage stability typically requires the inclusion of load dynamics in the modeling process [10]. Pump motors, in particular, consume a significant portion of the total power output from generators, typically ranging between 60% and 70%, due to their inherent inefficiencies. Consequently, the dynamic characteristics of system loads, specifically those associated with motors, play a crucial role in the overall system dynamics [11]. Numerous research studies have been conducted to investigate the stability of IMs [12, 13]. With recent advancements in this field, power electronic devices have become feasible, thanks to the widespread adoption of variable speed drives in various applications and the ability of inverters to modify the voltage at dc-link.

This research considers the mathematical modeling of an IM based on the synchronous reference frame. In a previous study [14], the state space model of the IM driving included the dynamic equations of dc-link voltage and currents. In [15], the authors conducted a study on the stability of an open loop Voltage/Frequency control for driving an IM using an inverter, and they also examined the influence of feedback. The stability of Voltage/Frequency control under dc voltage management was analyzed. In [16], the authors investigated how different parameters of the induction motor affect system stability. They also explored the impact of incorporating DC voltage as a coefficient of dq based current components in the stator current equation, considering solar and inverter irradiation fluctuations. Prior to discussing the tiny signal model, the non-linear model is presented in detail.

1) The proposed system's nonlinear model:

A) DC-link voltage control modeling:

The dynamic behavior of the dc-link voltage (V_{dc}) is illustrated in the table provided. This voltage is achieved through the current balancing mechanism of a capacitor.

$$V_{dc} = -\int (I_{IN} - I_{PV}) \frac{1}{C} dt \quad (1)$$

Where I_{PV} represents the PV-current and I_{IN} represents the current.

$$I_{IN} = \frac{P_{out}}{V_{dc}} \quad (2)$$

Consider that the system is completely efficient.

$$P_o = \omega \times T_e \quad (3)$$

Here, ω and T_e are the speed and torque of the motor.

$$T_e = \frac{3}{2}\frac{p}{2} L_m (i_{dr} i_{qs} - i_{qr} i_{ds}) \quad (4)$$

$$\omega = \frac{p}{2}\frac{1}{J}\int (T_e - T_L) dt \quad (5)$$

$$i_{ds} = \frac{\psi^*}{L_m} \quad (6)$$

$$i_{qs} = \frac{T_{en}}{\psi} \tag{7}$$

$$\psi = \sqrt{(\psi_d^2 + \psi_q^2} \tag{8}$$

Where $\psi_d = L_m(i_{ds} + i_{dr}) + L_{ls} i_{ds}$ & $\psi_q = L_m(i_{qs} + i_{qr}) + L_{ls} i_{qs}$

B) Non-linear approach of PV panels:

Output current of PV is

$$I_{PV} = \frac{V_d - V_{PV}}{R_s} \tag{9}$$

$$I_d = I_0 \left(e^{\frac{V_d}{V_t}} - 1 \right) \tag{10}$$

$$I_{ph} = G \times \frac{I_{sc}}{G^*} \tag{11}$$

By (1-11), the block diagram of the proposed system's nonlinear model can be produced, as illustrated in Fig 3..

$G_{dc}(s)$ and $G_{ac}(s)$ are controllers of dc-link and ac.

$$x = \frac{1}{v \times R_s}$$

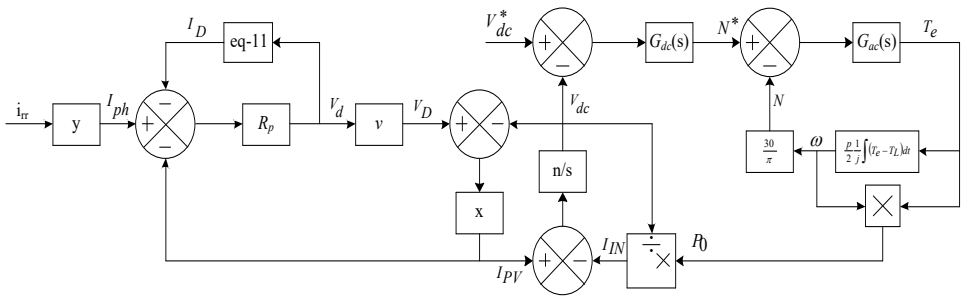

Fig. 3: Non-linear model.

2) Linear model:

In this study, basic mathematical equations are employed to attain the stability of a small signal in an inverter-controlled IM. The proposed model for water pumping is evaluated for stability analysis in a closed loop using a non-linear model depicted in Figure 3, which replicates the system shown in Figure 1.

A) Control of voltage at DC-Link and Vector Control.

The proposed system's miniature signal model, as illustrated in Figure 1, is obtained through the linearization of the entire model using differential equations. The linearization technique employed is based on the Taylor series expansion. The control system portrayed in Figure 3 is nonlinear, exhibiting a connection between the vector and dc-link voltage control loop. In normal operations, fluctuations in the voltage at dc-link as well as the current component of a quadrature axis (i_{qs}) can be utilized to construct the small signal model. In the proposed control method, the reference current for the direct axis component

of current (i_{ds}) is kept constant for the purpose of simplification. The equations given below are employed to produce the small signal model.

ΔV_{dc} can obtain by following equation:

$$\frac{1}{C}\int(\Delta I_{IN}-\Delta I_{PV})dt=-V_{dc}$$

Here, I_{IN} is computed using equations, hence,

$$\Delta I_{IN}=\frac{1}{V_{dc0}}\left[\Delta P_o-\frac{P_{o0}\times\Delta V_{dc}}{V_{dc0}}-\frac{\Delta P_o\times\Delta V_{dc}}{V_{dc0}}\right]$$

For simplicity, neglect $\frac{P_{out0}\times\Delta V_{dc}}{V_{dc0}^2}\approx 0$ higher order tiny signal components, as well as

$$\therefore \Delta I_{IN}=\frac{\Delta P_{out}}{V_{dc0}} \tag{12}$$

From the Figure 3:

$$N^*=(V_{dc}^*-V_{dc})\times G_{dc}(s)$$

Hence,

$$N^*=k_1(V_{dc}^*-V_{dc})\times PI_1$$

The following equations are used to calculate N* from the given equations:

$$\Delta N^*=k_1(\Delta V_{dc}^*-\Delta V_{dc})\times PI \tag{13}$$

From eq-7, Δi_{qs} can be developed as:

$$\Delta i_{qs}=\frac{1}{\psi_0}\left[\Delta T_{en}-\frac{T_{en0}\Delta\psi}{\psi_0}\right] \tag{14}$$

From eq-4, ΔT_e can be developed as:

$$\Delta T_e=\frac{3}{2}\frac{p}{2}L_m(\Delta i_{dr}\times i_{qs0}+\Delta iqs\times i_{dr0}-\Delta i_{qr}\times i_{ds}) \tag{15}$$

$$Ten=G_{ac}(s)\times(N^*-N)$$

$$Ten=k\times PI_2\times(N^*-N)$$

Then ΔT_{en} is obtained as:

$$\Delta Ten=k(\Delta N^*-\Delta N)\times PI_2 \tag{16}$$

$$i_{dr}=i_{ds}\cos\theta+i_{qs}\sin\theta$$

Δi_{dr} is:

$$\Delta i_{dr}=(i_{qs0}\cos\theta_0-i_{ds}\sin\theta_0)\Delta\theta+\sin\theta_0\Delta i_{qs} \tag{17}$$

$$\Delta i_{qr}=-(i_{ds}\cos\theta_0-i_{qs0}\sin\theta_0)\Delta\theta+\cos\theta_0\Delta i_{qs} \tag{18}$$

Where, $\Delta\theta=\frac{-i_{ds}\Delta i_{qs}}{i_{qs0}^2+i_{ds}^2}$

The following equations represent the small signal method of the quadrature and direct axis components of flux.

$$\Delta\psi_d = L_m \Delta i_{dr} \tag{19}$$

$$\Delta\psi_q = L_{ls}\Delta i_{qs} + L_m(\Delta i_{qs} + \Delta i_{qr}) \tag{20}$$

Thus,

$$\Delta\psi = \frac{1}{\psi_0}(\Delta\psi_{ds}\psi_{ds0} + \Delta\psi_{qs}\psi_{qs0}) \tag{21}$$

Then

$$\Delta\omega = \frac{p}{2}\frac{1}{J}\int(\Delta T_e - \Delta T_L)dt \tag{22}$$

$$\Delta P_0 = \Delta\omega T_{e0} + \Delta T_e \omega_0 \tag{23}$$

B)Small signal procedure:

$$\Delta I_d = I_0 \frac{\Delta V_d}{V_t} e^{\frac{V_{d0}}{V_t}} \tag{24}$$

$$\Delta I_{ph} = \Delta G \times \frac{I_{sc}}{G^*} \tag{25}$$

$$\Delta I_{PV} = \frac{\Delta V_d - \Delta V_{PV}}{R_s} \tag{26}$$

$$\Delta V_d = R_p\left(\Delta I_{ph} - \Delta I_{PV} - \Delta I_d\right) \tag{27}$$

$$\Delta P = \Delta\omega T_{e0} + \Delta T_e \omega_0 \tag{28}$$

Figure 4 constructed by using above basic equations:

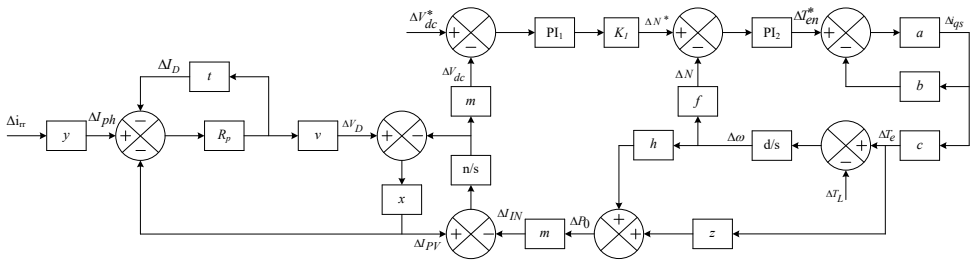

Fig. 4: Proposed method's linearized model.

5. DESIGN OF CONTROLLERS

The inner loop of the voltage/speed control of the IM is depicted in Fig. 4. This loop incorporates a PI2 controller and is illustrated in Fig. 5.

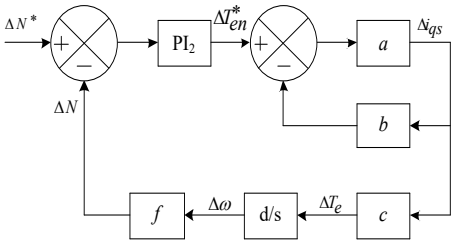

Fig. 5: Control loop for speed.

Thus, Figure 6 is derived from Figure 5. .

Here $K^1 = \dfrac{a.c.d.f}{(1+a.b)}$

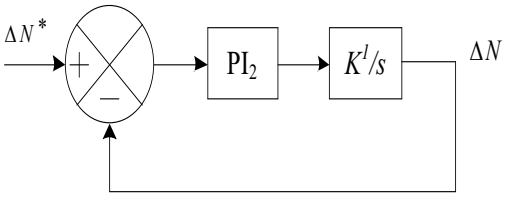

Fig. 6: Inner loop.

$$\frac{\Delta N}{\Delta N^*} = \frac{K^1 \times K_{p2}(s + \dfrac{K_{i2}}{K_{p2}})}{s^2 + (K^1 \times K2)s + K^1 \times K_{i2}} \tag{29}$$

Hence.

$$\frac{K^1 \times K_{p2}(s + \dfrac{K_{i2}}{K_{p2}})}{(s+\alpha)(s + \dfrac{K_{i2}}{K_{p2}} + \xi)} \tag{30}$$

Equations 29 and 30 can be compared to determine the decoupling between the inner and outer loops. It is recommended that the inner loop is designed to operate at a faster pace than the outer loop. The same objective can be achieved by following the approach demonstrated below.

$$K^1 \times K_{i2} = \alpha \times (\frac{K_{i2}}{K_{p2}} + \xi) \tag{31}$$

$$K^1 \times K_{p2} = \alpha + \frac{K_{i2}}{K_{p2}} + \xi \tag{32}$$

For fast response systems, the outer loop can be depicted in Figure 7.

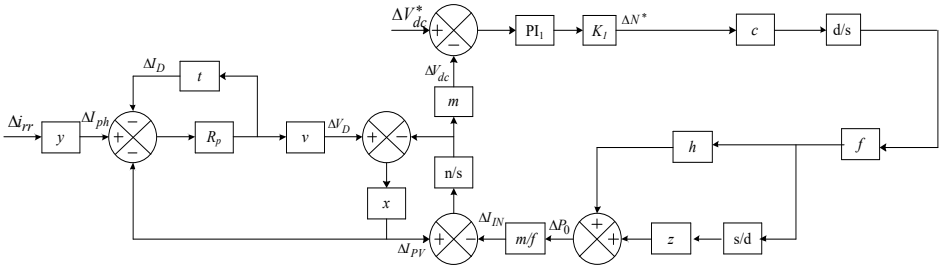

Fig. 7: outer loop.

Therefore,

$$\frac{\Delta V_{dc}}{\Delta i_{rr}} = \frac{K^{11} \times K_{p1}(s + a_1)}{s^2 + b_2 s + b_3} \tag{33}$$

Here, K^{11}, a_1, b_2 and b_3 are constants.

6. ANALYSIS AND RESULTS

The parameters of the IM and PV unit are obtained from references [16-21]. In Figure 8, the response of the voltage at dc-link is illustrated for a 20% variation in irradiance (at t=2.50sec.) for both the real model (Figure 1) and the linear model (Figure 4).

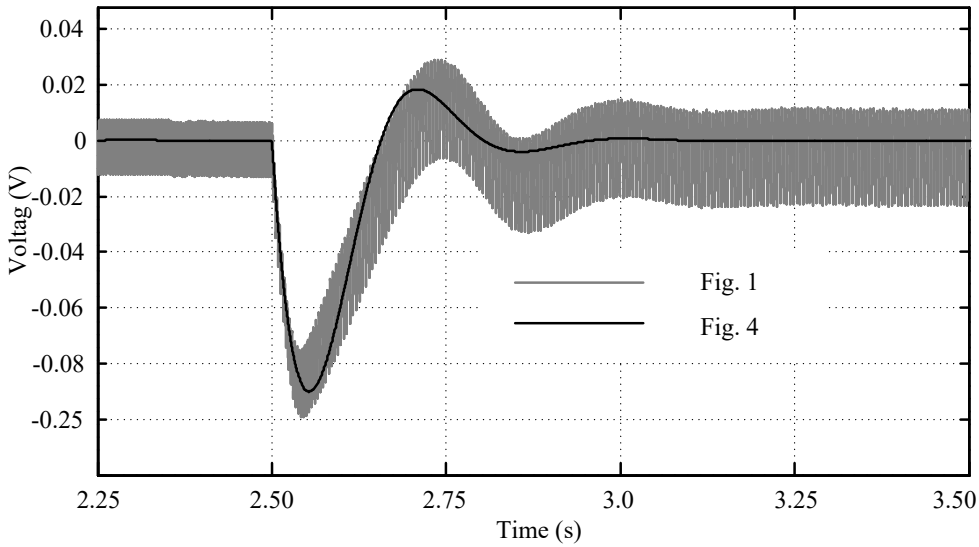

Fig. 8: Voltage at dc-link.

Therefore,

$$\frac{\Delta V_{dc}}{\Delta V_{dc}^*} = \frac{b_{21}s^3 + b_{22}s^2 + b_{23}s + b_{24}}{s^4 + d_{21}s^3 + d_{22}s^2 + d_{23}s + d_{24}} \tag{34}$$

A small signal based transfer function is given by equation 35, and response of function for a step change at t=1.0sec.(increased) and t=1.25(decreased) sec. is shown in Figure 9.

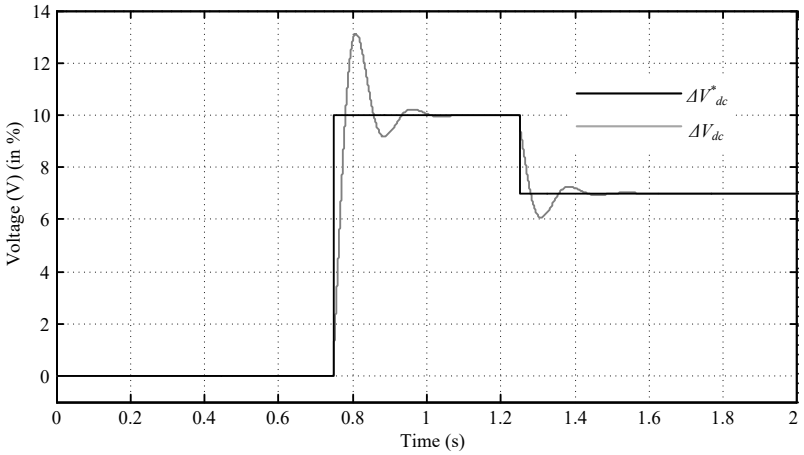

Fig. 9: profile of Voltage.

$$\Delta V_{dc} = \frac{b_{11}s^3 + b_{12}s^2 + b_{13}s}{s^4 + d_{11}s^3 + d_{12}s^2 + d_{13}s + d_{14}} \times \Delta irr + \frac{b_{21}s^3 + b_{22}s^2 + b_{23}s + b_{24}}{s^4 + d_{21}s^3 + d_{22}s^2 + d_{23}s + d_{24}} \times \Delta V^*_{dc} + \frac{-(b_{31}s^4 + b_{32}s^3 + b_{33}s^2)}{s^6 + d_{31}s^5 + d_{32}s^4 + d_{33}s^3 + d_{34}s^2 + d_{35}s + d_{36}} \times \Delta T_L \quad (35)$$

Where, b_{11}, b_{12}, b_{13}, b_{21}, b_{22}, b_{23}, b_{24}, b_{31}, b_{32}, b_{33}, d_{11}, d_{12}, d_{13}, d_{14}, d_{21}, d_{22}, d_{23}, d_{24}, d_{31}, d_{32}, d_{33}, d_{34}, d_{35} and d_{36} are constants.

The occurrence of equation 35's reaction becomes apparent as the sun's irradiation is diminished by 250% at t=3.0 sec and amplified by 250% at t=4.0 sec. Figure 10 illustrates the resultant change in nominal DC link voltage. The adjustments are constrained, and the system possesses the capability to regain its functionality despite this significant alteration.

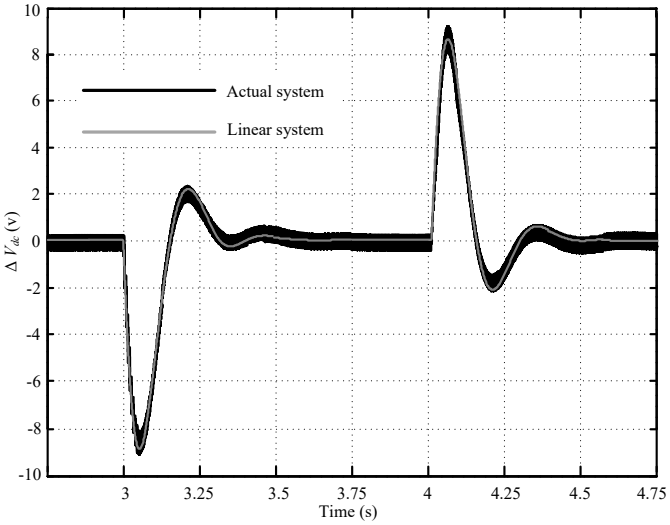

Fig. 10: Voltage response at dc-link.

7. CONCLUSIONS

A vector control technique is utilized in constructing a PV-operated WPS that operates independently without any batteries or storage system in this research. To enhance its responsiveness in the face of disturbances, a small signal analysis is conducted on the proposed approach. The responses of both the linearized and actual systems coincide, indicating that the transfer function can effectively depict the dynamic behavior of the model. The controller parameters are determined based on a conservative signal transfer function to ensure the desired system stability.

REFERENCES

[1] Malla Siva Ganesh et.al. "Coordinated power management and control of renewable energy sources based smart grid" International Journal of Emerging Electric Power Systems, vol. 23, no. 2, 2022, pp. 261-276. https://doi.org/10.1515/ijeeps-2021-0113.

[2] C. Pradhan, M. K. Senapati, S. G. Malla, P. K. Nayak and T. Gjengedal, "Coordinated Power Management and Control of Standalone PV-Hybrid System With Modified IWO-Based MPPT," in IEEE Systems Journal, vol. 15, no. 3, pp. 3585-3596, Sept. 2021, doi: 10.1109/JSYST.2020.3020275..

[3] S. R. Bhat, Andre Pittet and B. S. Sonde, "Performance Optimization of Induction Motor-Pump System Using Photovoltaic Energy Source", *IEEE Transactions on Industry Applications*, Vol. IA-23, No. 6, Nov/Dec. 1987.

[4] S. G. Malla et al., "Whale Optimization Algorithm for PV Based Water Pumping System Driven by BLDC Motor Using Sliding Mode Controller," in IEEE Journal of Emerging and Selected Topics in Power Electronics, vol. 10, no. 4, pp. 4832-4844, Aug. 2022, doi: 10.1109/JESTPE.2022.3150008..

[5] Bhende, Chandrashekhar N. and Malla, Siva G.. "Novel Control of Photovoltaic based Water Pumping System without Energy Storage" International Journal of Emerging Electric Power Systems, vol. 13, no. 5, 2012. https://doi.org/10.1515/1553-779X.2931.

[6] B. B. Rath et al., "Photovoltaic Partial Shading Performance Evaluation With a DSTATCOM Controller," in IEEE Access, vol. 10, pp. 69041-69052, 2022, doi: 10.1109/ACCESS.2022.3186906.

[7] J. R. Arribas and C. M. V. González, "Optimal vector control of pumping and ventilation induction motor drives," *IEEE Transactions on Industrial Electronics*, Vol. 49, pp. 889–895, Aug. 2002.

[8] G. R. Whitfield, R. W. Bentley, and J. D. Burton, "Increasing the cost effectiveness of small solar photovoltaic pumping systems", *Renewable Energy*, Vol. 6, pp. 483–486, 1995.

[9] Mohammed Ali Elgendy, Bashar Zahawi and David John Atkinson, "Comparison of Directly Connected and Constant Voltage Controlled Photovoltaic Pumping Systems", *IEEE Transactions on Sustainable Energy*, Vol. 1, No. 3, Oct 2010.

[10] R. H. Lasseter and P. Paigi, "Microgrid: a conceptual solution," 2004 IEEE 35th Annual Power Electronics Specialists Conference (IEEE Cat. No.04CH37551), 2004, pp. 4285-4290 Vol.6, doi: 10.1109/PESC.2004.1354758. .

[11] Prabha Kundur, "Power System Stability and Control" New York: McGraw-Hill, 1994

[12] Paul C. Krause, Oleg Wasynczuk, Scott D. Sudhoff, "Analysis of electric machinery and drive systems" New York, John Wiley & Sons Inc., 2002.

[13] R. Krishnan, "Electric motor drives : modeling, analysis, and control", Upper Saddle River, NJ : Prentice Hall, 2001.

[14] A. D. Del Rosso, Mariano Anello, E. Spittle, “Stability Assessment of Isolated Power Systems with Large Induction Motor Drives” *IEEE Transmission & Distribution Conference and Exposition*: Latin America, 2006
[15] Suzuki, K.; Saito, S.; Kudor, T.; Tanaka, A.; Andoh, Y. “Stability Improvement of V/F Controlled Large Capacity Voltage-Source Inverter Fed Induction Motor” *IEEE Industry Applications Conference*, 2006.
[16] Yunjun Guo; Dong Wang; Dezhi Liu; Junquan Chen, “Small Disturbance Stability Analysis of Multiphase Inverter-fed Induction Motor Drive System” XIX International Conference on Electrical Machines - ICEM 2010, Rome, 2010.
[17]. Priyanka Malla, “TSK Fuzzy Controller for Vector Control of Induction Motor”, International Journal of New Technologies in Science and Engineering (IJNTSE), Vol. 8, Issue. 1, pp. 1-5, Jan. 2022.
[18]. U. R. Muduli, B. Chikondra, M. J. Akhtar, O. Al Zaabi, K. Al Hosani and R. K. Behera, "Comparison of SVPWM Techniques Under Switching Loss Control for Induction Motor Drive With LC Filters," in IEEE Transactions on Industry Applications, doi: 10.1109/TIA.2022.3231841.
[19]. U. R. Muduli, R. K. Behera, K. Al Hosani and M. S. E. Moursi, "Direct Torque Control With Constant Switching Frequency for Three-to-Five Phase Direct Matrix Converter Fed Five-Phase Induction Motor Drive," in IEEE Transactions on Power Electronics, vol. 37, no. 9, pp. 11019-11033, Sept. 2022, doi: 10.1109/TPEL.2022.3167477.
[20]. O N Chandrasekhar, “Modified Grey Wolf Optimization Algorithm for MPPT of PV System under Partial Shading Conditions”, International Journal of New Technologies in Science and Engineering (IJNTSE), Vol. 8, Issue. 5, pp. 1-6, May. 2022.
[21]. U. R. Muduli, K. A. Hosani, K. A. Jaafari, J. Y. Alsawalhi, A. S. Al-Sumaiti and R. K. Behera, "ANN based On-board Fault Diagnostic for Induction Motor Drive in Low-Cost Electric Vehicles," 2022 IEEE Applied Power Electronics Conference and Exposition (APEC), Houston, TX, USA, 2022, pp. 153-158, doi: 10.1109/APEC43599.2022.9773566.